Monthly Notices of the ROYAL ASTRONOMICAL SOCIETY
MNRAS **470,** 2791–2798 (2017)
Advance Access publication 2017 June 7
doi:10.1093/mnras/stx1386

Introducing the FirstLight project: UV luminosity function and scaling relations of primeval galaxies

Daniel Ceverino,⋆ Simon C. O. Glover and Ralf S. Klessen
Institut für Theoretische Astrophysik, Zentrum für Astronomie, Universitiät Heidelberg, Albert-Ueberle-Str. 2, D-69120 Heidelberg, Germany

Accepted 2017 June 2. Received 2017 May 30; in original form 2017 March 8

ABSTRACT

We introduce the FirstLight project, which aims to generate a large data base of high-resolution, zoom-in simulations of galaxy formation around the epoch of reionization ($z \geq 6$). The first results of this programme agree well with recent observational constraints at $z = 6$–8, including the ultraviolet (UV) luminosity function and galaxy stellar mass function, as well as the scaling relationships between halo mass, stellar mass and UV magnitude. The UV luminosity function starts to flatten below $M_{\rm UV} > -14$ due to stellar feedback in haloes with maximum circular velocities of $V = 30$–40 km s^{-1}. The power-law slope of the luminosity function evolves rapidly with redshift, reaching a value of $\alpha \simeq -2.5$ at $z = 10$. On the other hand, the galaxy stellar mass function evolves slowly with time between $z = 8$ and 10, in particular, at the low-mass end.

Key words: galaxies: evolution – galaxies: formation – galaxies: high-redshift.

1 INTRODUCTION

The formation of the first stars and galaxies marks the beginning of the cosmic dawn, when stellar light spreads across the cosmos. The first light of these primeval galaxies reshapes the global properties of the Universe during the epoch of reionization. However, very little is known about the properties of galaxies during the first billion years of the Universe.

One of the basic properties during the reionization epoch is the abundance of galaxies as a function of their ultraviolet (UV) luminosities. The shape and evolution of the UV luminosity function (UVLF) gives insight into the efficiency of star formation as a function of halo mass and time. This is crucial for assessing the importance of galaxies for the reionization of the Universe. Surveys from *Hubble Space Telescope* (*HST*) fields have yielded a large population of galaxies between redshifts $z = 4$ and 10 (Bouwens et al. 2004; Finkelstein et al. 2012; Oesch et al. 2013; Bouwens et al. 2015). This allows the accurate determination of the UVLF at $z \leq 8$ and its evolution. Observations indicate a decrease in the normalization with increasing redshift, as well as a steepening of the low-luminosity slope. However, large uncertainties remain at higher redshifts ($z \geq 10$), as well as at the high- and low-luminosity ends ($M_{\rm UV} < -22$ and $M_{\rm UV} > -16$), due to the low number of observed galaxies. Future deep surveys using the *James Webb Space telescope* (*JWST*) will significantly improve this situation. Meanwhile, theoretical predictions are crucial for the design of these future surveys.

Any theory of galaxy formation should predict the right correlations between three basic galaxy properties: the mass of a halo (or its virial mass, $M_{\rm vir}$), the stellar mass of the galaxy at the centre of this halo (M_*), and the star formation rate (SFR) or the equivalent UV magnitude ($M_{\rm UV}$) within the galaxy. Observations are starting to constrain these scaling relations at high z (Stark et al. 2013; Duncan et al. 2014; Song et al. 2016; Stefanon et al. 2016). Taking into account the nebular emission lines, current determinations of the $M_{\rm UV}$–M_* relation at different redshifts show a weak evolution with time. However, the uncertainties are still large. The galaxy stellar mass function has also been measured at $4 < z < 8$ (Song et al. 2016; Stefanon et al. 2016), and these observations report a steep low-mass end, although its evolution is a matter of debate.

Many theoretical studies predict a flattening or turnover in the UVLF at low luminosities (Jaacks, Thompson & Nagamine 2013; Dayal et al. 2014; Boylan-Kolchin et al. 2015; Gnedin 2016). However, a disagreement remains about the details of this flattening. For example, Gnedin (2016) and Liu et al. (2016) report a break for $M_{\rm UV} > -12$ due to a decrease in the efficiency of cooling processes in low-mass haloes, while Jaacks et al. (2013) find a turnover at $M_{\rm UV} \simeq -15$. Other proposed mechanisms include a greater role of radiative feedback that quenches star formation in haloes below a given circular velocity of 30–50 km s^{-1} (O'Shea et al. 2015; Ocvirk et al. 2016; Yue, Ferrara & Xu 2016).

Due to the importance of the UVLF, the scaling relations between halo mass, stellar mass and SFR have received less attention, particularly in the regimes where there are observational constraints. Some exceptions include the M_*—SFR relation (Cullen et al. 2017; Pawlik et al. 2017), and the $M_{\rm UV}$–$M_{\rm vir}$ relation (Liu et al. 2016; Finlator et al. 2017), where simulations tend to overproduce stars

⋆ E-mail: ceverino@uni-heidelberg.de

in comparison with simple models of abundance matching (Finkelstein et al. 2015).

The FirstLight project is motivated by the need for a large, statistically significant sample of galaxies simulated at very high resolution at the epoch of reionization ($z \geq 6$). Current simulations of galaxy formation at these redshifts yield a large population of galaxies in large volumes, but the internal properties of their interstellar medium are poorly resolved (Genel et al. 2014; Pawlik et al. 2017) and rely heavily on subgrid modelling. On the other hand, current zoom-in simulations (Ma et al. 2015; Fiacconi et al. 2017; Pallottini et al. 2017) concentrate all the computational resources in one or just a few galaxies with much higher resolution. However, the small sample makes them very sensitive to selection effects and poor statistics.

The FirstLight project is the largest sample of zoom-in, initial conditions carried out to date that will reach typical resolutions of about 10 pc in volumes of up to ~60 Mpc. Such a large programme, first, needs a validation test. We need to make sure that simulated galaxy properties, in particular, halo mass, stellar mass and SFR, are consistent with the observed luminosity and galaxy mass function, as well as the scaling relations constrained by observations and other independent methods, such as abundance matching (Behroozi & Silk 2015).

The outline of this paper is as follows. Section 2 describes the full FirstLight sample, as well as the simulations details and the initial conditions of the zoom-in simulations that comprise the test runs. Section 3 describes the results of the FirstLight tests at $z = 6$. The following sections are devoted to the evolution of the SMHM relation (Section 4): the UVLF (Section 5) and the galaxy stellar mass (Section 6). Section 7 finishes with the conclusion and final discussions.

2 THE SIMULATIONS

2.1 The FirstLight sample

The FirstLight project consists of a mass-limited sample of haloes with a maximum circular velocity, V, between 50 and 250 km s^{-1}, selected at $z = 5$. The sample covers a halo mass range between a few times 10^9 M$_\odot$ and a few times 10^{11} M$_\odot$. This range excludes massive and rare haloes with number densities lower than $\sim 10^{-4}\, h^{-1}$ Mpc^{-3}, as well as small haloes in which galaxy formation is extremely inefficient.

The sample uses two different sets of cosmological parameters: *Wilkinson Microwave Anisotropy Probe* (*WMAP5*) with $\Omega_m = 0.27$, $\Omega_b = 0.045$, $h = 0.7$ and $\sigma_8 = 0.82$ (Komatsu et al. 2009), and *Planck13* results (Planck Collaboration XVI 2014) with $\Omega_m = 0.307$, $\Omega_b = 0.048$, h = 0.678 and $\sigma_8 = 0.823$. This allows us to compare the effects of the different cosmological parameters on the formation of first galaxies. In particular, the value of Ω_m in the *Planck* cosmology is significantly higher than the *WMAP* value, commonly used in previous simulations.

We employ a standard zoom-in technique (Klypin, Zhao & Somerville 2002) to generate the initial conditions. For each set of cosmological parameters, we have three different cosmological boxes of 10, 20 and 40 h^{-1} Mpc. For each box, we first run a low-resolution (128^3 particles) N-body-only simulation ($z_{\rm init} = 150$) with the ART code (Kravtsov, Klypin & Khokhlov 1997). We select all distinct haloes with a maximum circular velocity at $z = 5$ greater than a specified threshold $V_{\rm cut}$ (Table 1). This restriction allows us to avoid including poorly resolved haloes in our sample. The main sample consists of 978 haloes.

Table 1. The FirstLight sample. The units for box size and $V_{\rm cut}$ are h^{-1} Mpc and km s^{-1}, respectively.

Box size	Cosmology	Effective resolution	log($V_{\rm cut}$)	# of haloes
10	*WMAP*	2048^3	1.7	201
20	*WMAP*	4096^3	2.0	114
40	*WMAP*	8192^3	2.3	31
10	*Planck*	2048^3	1.7	344
20	*Planck*	4096^3	2.0	228
40	*Planck*	8192^3	2.3	60

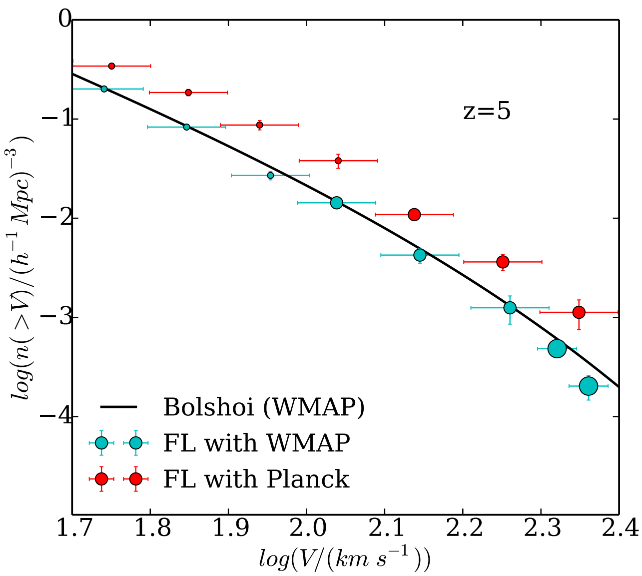

Figure 1. Velocity function of DM haloes from the FirstLight sample at $z = 5$. The size of the points increases with box size (Table 1). The results with a *WMAP* cosmology are consistent with the halo statistics from the Bolshoi simulation (Klypin, Trujillo-Gomez & Primack 2011) using the same cosmological parameters. By contrast, the halo number densities with *Planck* cosmology are significantly higher due to the higher Ω_m value.

Using these haloes, we generate the velocity function at $z = 5$ (Fig. 1) and compare it with the results coming from large N-body-only simulations, such as the Bolshoi simulation (Klypin et al. 2011) with a box size of 250 h^{-1} Mpc. The halo statistics with *WMAP* cosmology are remarkably similar to Bolshoi, which uses the same cosmological parameters. This demonstrates that the halo number densities are accurately reproduced within the selected mass range, despite the relatively small cosmological volumes and the low resolution used in the selection of haloes. Higher resolution runs with 256^3 particles confirm that these results have converged.

The halo statistics with *Planck* cosmology show significantly higher halo number densities. This is a consequence of the higher Ω_m from *Planck* with respect to *WMAP*. In a more massive Universe, structures collapse earlier and they are denser. For example, the number density of distinct haloes at $z \simeq 7$ increases by a factor of 1.5−3, depending on their mass (Rodríguez-Puebla et al. 2016). This could have important implications for the formation of the first galaxies and reionization.

Once the haloes are selected, the initial conditions with higher resolution are generated using PMGALAXY (Klypin et al. 2011) for the 10 and 20 h^{-1} Mpc boxes and using MUSIC (Hahn & Abel 2011) for the 40 h^{-1} Mpc box. All three volumes have the same dark matter (DM) particle mass resolution of $m_{\rm DM} = 10^4$ M$_\odot$ (a maximum effective resolution of 8192^3 particles). The minimum mass of star particles is 100 $M_\odot$. The maximum spatial resolution is always between 8.7 and 17 proper pc (a comoving resolution of 109 pc after $z = 11$). This mass resolution is a factor of 3 better than in the Renaissance simulations (O'Shea et al. 2015) and comparable to the resolution in the FiBY project (Paardekooper, Khochfar & Dalla Vecchia 2013; Cullen et al. 2017) but in a much larger volume.

2.2 ART

The simulations are performed with the ART code (Kravtsov et al. 1997; Kravtsov 2003), which accurately follows the evolution of a gravitating *N*-body system and the Eulerian gas dynamics using an Adaptive Mesh Refinement (AMR) approach. Besides gravity and hydrodynamics, the code incorporates many of the astrophysical processes relevant to galaxy formation. These processes, representing subgrid physics, include gas cooling due to atomic hydrogen and helium, metal and molecular hydrogen cooling, photoionization heating by a constant cosmological UV background with partial self-shielding, star formation and feedback, as described in Ceverino & Klypin (2009), Ceverino, Dekel & Bournaud (2010) and Ceverino et al. (2014).

In addition to thermal-energy feedback, the simulations use radiative feedback, as a local approximation of radiation pressure. This model adds non-thermal pressure to the total gas pressure in regions where ionizing photons from massive stars are produced and trapped. In the current implementation, named RadPre_IR in Ceverino et al. (2014), radiation pressure is included in the cells (and their six closest neighbours) that contain stellar particles younger than 5 Myr and whose gas column density exceeds 10^{21} cm^{-2}. Finally, the model also includes a moderate trapping of infrared photons, only if the gas density in the host cell exceeds a threshold of 300 cm^{-3}. More details can be found in Ceverino et al. (2014).

In addition to radiative feedback, the latest model also includes the injection of momentum coming from the (unresolved) expansion of gaseous shells from supernovae and stellar winds (Ostriker & Shetty 2011). A momentum of 3×10^5 $M_\odot$ km s^{-1} per massive star (i.e per star more massive than 8 $M_\odot$) is injected at a constant rate over 40 Myr, the lifetime of the lightest star that explodes as a core-collapsed supernova. The resulting specific momentum when integrated over the initial mass function (IMF) is 3.75×10^3 km s^{-1}. The injection of momentum is implemented in the form of a non-thermal pressure, as in Ceverino et al. (2014).

This feedback model differs from other recent implementations. It goes beyond the thermal-only feedback (Stinson et al. 2006, 2013; Schaye et al. 2015), and it does not shut down cooling in the star-forming regions. It does not impose a wind solution (Hopkins et al. 2014; Vogelsberger et al. 2014), so that outflows are generated in a self-consistent way (Ceverino et al. 2016). Our implementation is more similar to the feedback model in Agertz & Kravtsov (2015). Within our model, both radiative feedback and supernova feedback act in concert and they are equally important. The combination of early feedback from radiation and late feedback from supernovae regulates star formation within galaxies (Ceverino et al. 2014).

2.3 FirstLight tests

As a feasibility study for this project, we generate the initial conditions for 15 haloes using the *WMAP* cosmology (Table 2). They cover the full range of halo masses of the FirstLight project, from $M_{\rm vir} \simeq 10^9$ to 10^{11} $M_\odot$ at $z = 5$. These are the simulations analysed in this paper. In order to avoid poorly resolved haloes, we restrict our analysis to haloes with $M_{\rm vir} \geq 10^9$ $M_\odot$. They contain more than ~8×10^4 DM particles within the virial radius. The runs finish at $z = 6$ when the analysis of the next section is performed, with the exception of the computationally most expensive run (FL21), which finishes at $z = 8$.

Table 2. Zoom-in simulations analysed in this paper as tests of the FirstLight project. Values are computed at $z_{\rm last} = 6$, unless otherwise stated. The units of the maximum circular velocity, *V*, virial mass, $M_{\rm vir}$, galaxy stellar mass, M_*, and rest-frame UV magnitude, $M_{\rm UV}$, are km s^{-1}, $M_\odot$ and mag, respectively.

ID	log[$V(z=5)$]	$z_{\rm last}$	$M_{\rm vir}/10^{10}$	$M_*/10^7$	$M_{\rm UV}$
FL01	1.60	6	0.11	0.14	−12.2
FL02	1.70	6	0.22	0.15	−11.9
FL04	1.72	6	0.47	0.48	−14.3
FL05	1.90	6	0.22	0.30	−13.6
FL06	1.97	6	0.28	0.32	−12.3
FL08	1.88	6	1.7	4.5	−16.7
FL11	1.96	6	2.5	13	−17.1
FL12	1.90	6	0.71	0.83	−15.0
FL13	1.84	6	0.64	2.9	−15.6
FL14	1.78	6	0.30	0.27	−13.5
FL15	1.70	6	0.36	0.62	−14.4
FL16	2.19	6	6.5	75	−18.9
FL17	2.15	6	6.1	89	−19.3
FL19	2.05	6	4.4	66	−19.0
FL21	2.38	8	0.26	0.37	−13.9

3 FIRSTLIGHT TESTS AT $z = 6$

First, we analyse the FirstLight tests at redshift $z = 6$, because there are many good observational constraints at that redshift. In order to estimate the UVLF from a set of zoom-in simulations, we need to compute the rest-frame UV magnitude associated with each major progenitor of the haloes selected in Section 2.3 (one galaxy per zoom-in), as well as the number density of haloes of the same mass as the progenitor. Our fundamental assumption here is that each object is an unbiased representative of a sample of galaxies with similar properties. The full FirstLight sample will further constrain the mean and scatter around these values.

The UV continuum emission ($L_{\rm UV}$) from a galaxy is proportional to its SFR, and it is independent of the galaxy history if it is measured at time-scales much longer than ~2×10^7 yr, the typical lifetime of late-O/early-B stars that dominate the UV continuum (Kennicutt 1998; Madau, Pozzetti & Dickinson 1998). Assuming a broad-band filter centred at 1500 Å with a bandpass width, $\Delta\lambda/\lambda = 0.2$, the UV luminosity becomes

$$L_{\rm UV} = \frac{\rm SFR}{M_\odot\ {\rm yr}^{-1}} 8 \times 10^{27} {\rm erg\ s^{-1}\ Hz^{-1}}, \quad (1)$$

where SFR is measured in a period of 3×10^8 yr. Using a shorter period of 10^8 yr introduces fluctuations in the UV magnitude due to the particular star formation histories of the FirstLight tests. These fluctuations add a maximum scatter of one magnitude around the UV magnitude measured with a period of 3×10^8 yr. We use the longer period because we are interested in the averaged UV luminosities, independent of their particular histories. The full FirstLight sample will allow us to characterize the diversity of star formation bursts and the variations in the UV magnitude in future work. We assume a Salpeter IMF and neglect the effects of dust absorption, which should be a good approximation for the primeval galaxies considered here (Bouwens et al. 2016b). Assuming a standard

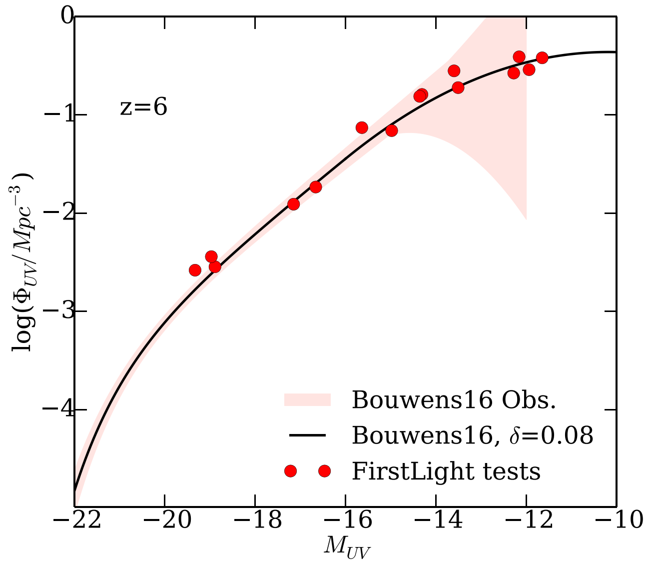

Figure 2. UVLFat $z = 6$. The FirstLight tests are consistent with observations (Bouwens et al. 2016a). They predict a progressive flattening of the LF at low luminosities ($M_{\rm UV} > -14$) driven by stellar feedback.

conversion to AB magnitudes (Bouwens et al. 2008), the UV magnitude becomes

$$M_{\rm UV} = -21.91 - 2.5\log\left(\frac{L_{\rm UV}}{2.5\times10^{29}\,{\rm erg\,s^{-1}\,Hz^{-1}}}\right). \quad (2)$$

The comoving number density is obtained from the maximum circular velocity (V) of the halo hosting each galaxy. It can be parametrized by the following expression (Klypin et al. 2011) coming from a large N-body simulation:

$$\Phi = AV^{-3}\exp\left(-(V/V_0)^{\alpha_{\rm H}}\right), \quad (3)$$

where $A = 2.8 \times 10^4\,({\rm Mpc\,km^{-1}\,s})^{-3}$, $\alpha_{\rm H} = 1.19$ and $V_0 = 79\ {\rm km\,s^{-1}}$ are the parameters described in Klypin et al. (2011) at $z = 6$, adapted to a *Planck* cosmology (Rodríguez-Puebla et al. 2016).

The FirstLight LF extends from high ($M_{\rm UV} \simeq -19$) to very low ($M_{\rm UV} \simeq -12$) luminosities (Fig. 2). It is consistent with recent observations that are able to reach such low luminosities, thanks to gravitational lensing (Bouwens et al. 2016a). In particular, the results predict a progressive flattening of the UVLF at low luminosities ($M_{\rm UV} > -14$). They can be parametrized by a modified version of the Schechter function (Bouwens et al. 2016a),

$$\Phi_{\rm UV} = \Phi^*\left(\frac{\ln(10)}{2.5}\right)10^{-0.4(M_{\rm UV}-M^*)(\alpha+1)e^{-10^{-0.4(M_{\rm UV}-M*)}}}f, \quad (4)$$

which includes a flattening factor for magnitudes fainter than $M_{\rm f} = -16$:

$$f = \begin{cases} 10^{-0.4\delta(M_{\rm UV}+M_{\rm f})^2} & \text{if } M_{\rm UV} \geq M_{\rm f} \\ 1 & \text{if } M_{\rm UV} < M_{\rm f} \end{cases}. \quad (5)$$

Our value for the curvature parameter, $\delta = 0.08 \pm 0.01$, is very similar to the mean parametric value used for the fiducial observations in Bouwens et al. (2016a): $\delta = 0.11 \pm 0.20$. The other parameters are the same as in Bouwens et al. (2016a). See Table 3.

This flattening of the UVLF is produced by the progressive inefficiency of star formation at lower halo masses (higher abundances) with maximum circular velocities of $V = 30$–$40\ {\rm km\,s^{-1}}$. At these masses, stellar feedback is able to quench star formation by heating

Table 3. Best parameters of the Schechter fit to the simulated UVLF. Fixed values come from Bouwens et al. (2016a).

z	α	$M^\star$	$\Phi^\star/10^{-3}\,{\rm Mpc^{-3}}$
6	−1.92	−20.94	0.57
8	−2.02	−20.63	0.21
10	−2.65 ± 0.15	−20.92	0.008 ± 0.005

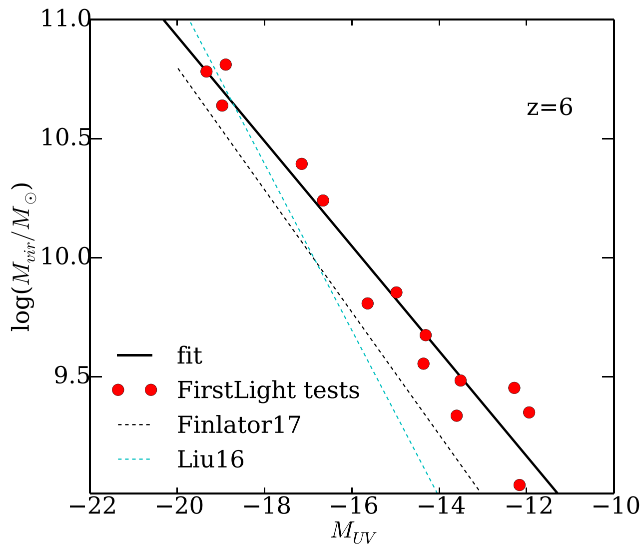

Figure 3. Virial mass versus rest-frame UV absolute magnitude at $z = 6$. Other recent simulations (Liu et al. 2016; Finlator et al. 2017) predict lower halo masses at a fixed UV magnitude for magnitudes fainter than $M_{\rm UV} = -18$.

and ejecting gas that would otherwise form stars at a rate set by the cosmological gas accretion rate (Dekel et al. 2013). Feedback is therefore able to decrease the SFR within these small galaxies, yielding UV magnitudes fainter than expected. This generates a flattening of the UVLF.

The above LF implies a specific scaling relation between the virial mass of the hosting halo and the galaxy UV magnitude (Fig. 3). For the luminosities sampled in this paper, the halo mass ranges between $M_{\rm vir} \simeq 10^9$ and $10^{11}\,{\rm M_\odot}$ at $z = 6$. The relation can be fitted by the following expression:

$$\left(\frac{M_{\rm vir}}{10^9\,{\rm M_\odot}}\right) = 10^{\alpha_{\rm v}(M_{\rm UV}-M^*_{\rm v})}, \quad (6)$$

where $\alpha_{\rm v} = -0.2204 \pm 0.0015$ and $M^*_{\rm v} = -11.27 \pm 0.02$. Other recent simulations (Liu et al. 2016; Finlator et al. 2017) predict brighter UV magnitudes for the same halo mass, especially for haloes less massive than $10^{10.5}\,{\rm M_\odot}$. Therefore, they produce too many stars. This is related to the different feedback models used in these simulations. When feedback is not able to properly regulate the star formation process in low-mass haloes, the simulation suffers from the overcooling problem that plagues many simulations of galaxy formation.

The relation between stellar mass and UV magnitude is another basic scaling relation (Fig. 4). The FirstLight results can be fitted by the following expression:

$$\left(\frac{M_*}{10^6\,{\rm M_\odot}}\right) = 10^{\alpha_*(M_{\rm UV}-M^*_*)}, \quad (7)$$

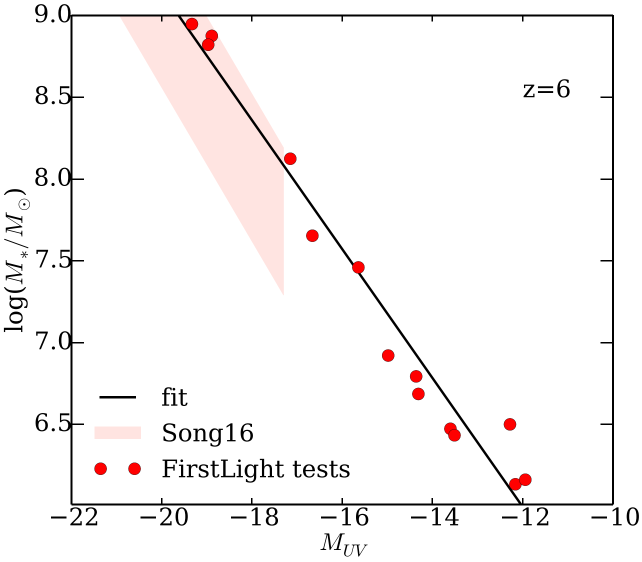

Figure 4. Stellar mass versus rest-frame UV absolute magnitude at $z = 6$. The FirstLight tests are consistent with current observations (Song et al. 2016) at high luminosities ($M_{\rm UV} < -18$).

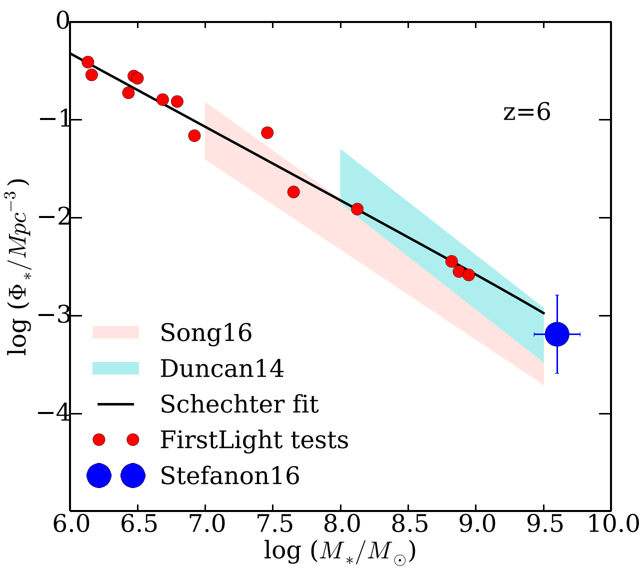

Figure 5. Stellar mass function at $z = 6$. FirstLight results are consistent with current observations (Duncan et al. 2014; Song et al. 2016; Stefanon et al. 2016) for $M_* > 10^7$ M$_\odot$. For lower masses, they predict a steep mass function without signs of flattening.

where $\alpha_* = -0.394 \pm 0.002$ and $M^*_* = -12.13 \pm 0.03$. The results at high luminosities ($M_{\rm UV} < -18$) are consistent with current observations (Song et al. 2016). The simulations contain the correct amount of stars for a given UV luminosity. Moreover, they continue the observed trend towards lower luminosities.

The stellar mass function (Fig. 5) is also consistent with recent observations (Duncan et al. 2014; Song et al. 2016; Stefanon et al. 2016) for $M_* > 10^7$ M$_\odot$. The highest mass bin around $M_* \simeq 10^9$ M$_\odot$ has an abundance that is somewhat on the high side of the observed range constrained by Song et al. (2016). It has a better agreement with the results by Duncan et al. (2014) and with observations using the LF in the rest-frame visible light (Stefanon et al. 2016). Therefore, the low-mass slope, $\alpha_s = -1.750 \pm 0.004$, is slightly shallower than the observational estimates (-1.91 ± 0.09) by Song et al. (2016):

Table 4. Best parameters of the Schechter fit to the simulated galaxy stellar mass function. Fixed values come from Bouwens et al. (2016a).

z	α_s	M^*_s	$\Phi^*_s/10^{-5}$ Mpc^{-3}
6	-1.75 ± 0.04	10.72	6.0 ± 0.4
8	-1.85 ± 0.04	10.72	1.3 ± 0.4
10	-1.84 ± 0.12	10.72	0.95 ± 1

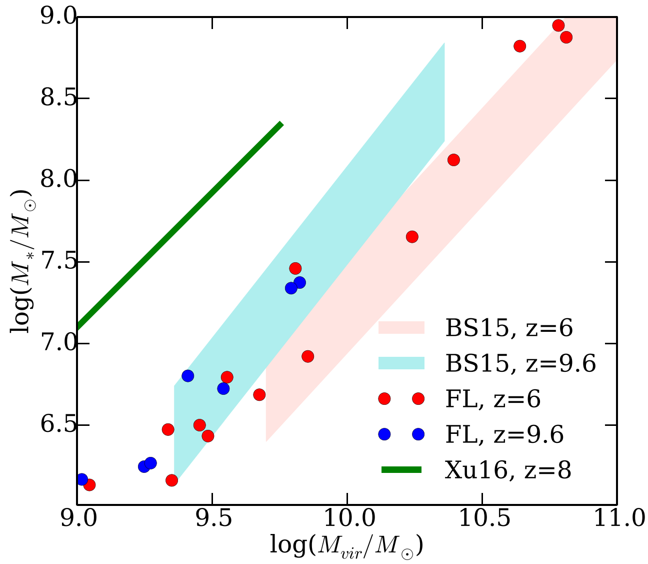

Figure 6. Evolution of the SMHM relation between $z = 9.6$ and 6. The simulations are consistent with the evolution predicted by abundance matching models (Behroozi & Silk 2015). The Renaissance simulation (Xu et al. 2016) forms many more stars by an order of magnitude.

$$\Phi_* = \Phi^*_s \ln(10) 10^{(M-M^*_s)(\alpha_s+1)} e^{-10^{(M-M^*_s)}}, \tag{8}$$

where $M = \log(M_*)$. The parameters of the Schechter fit are shown in Table 4. The parameter M^*_s is fixed to the value reported in Song et al. (2016) because the FirstLight tests do not extend to high masses and they cannot constrain the exponential drop-off. For stellar masses lower than 10^7 M$_\odot$, the simulations do not show any sign of flattening of the mass function.

4 EVOLUTION OF THE STELLAR-TO-HALO MASS RELATION

A crucial check in cosmological simulations of galaxy formation is the SMHM ratio (Fig. 6). Model galaxies should live in haloes of the right mass because many properties, such as the gas accretion rate, depend on the halo mass. However, it is difficult to measure the halo mass observationally. Therefore, we often compare with independent semi-empirical models such as abundance matching (Behroozi, Wechsler & Conroy 2013; Moster, Naab & White 2013).

After excluding a couple of outliers, the FirstLight simulations are consistent with the evolution predicted by abundance matching models (Behroozi & Silk 2015). Between $z = 6$ and 10, we found a normalization shift of about 0.5 dex at $M_{\rm vir} \simeq 10^{10}$ M$_\odot$. This shift is linked to differences between the evolution of the halo and galaxy mass functions. Haloes grow faster than galaxies, which are

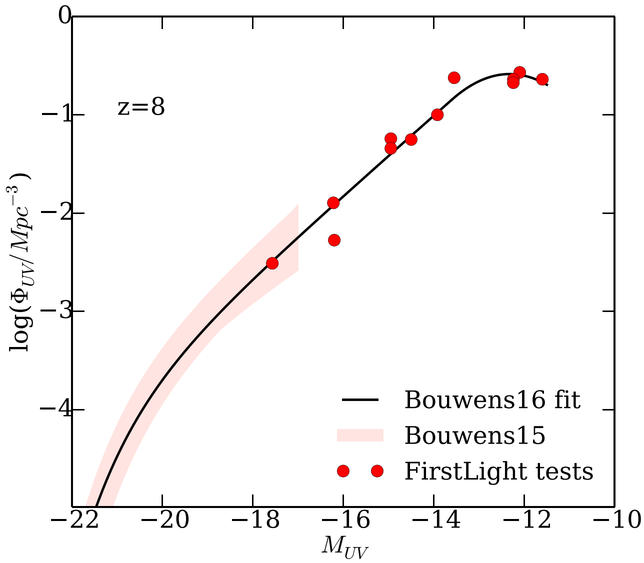

Figure 7. UVLF at $z = 8$. The FirstLight results are consistent with the extrapolation of the observed results (Bouwens et al. 2015) with a strong flattening at low luminosities ($M_{\rm UV} > -14$).

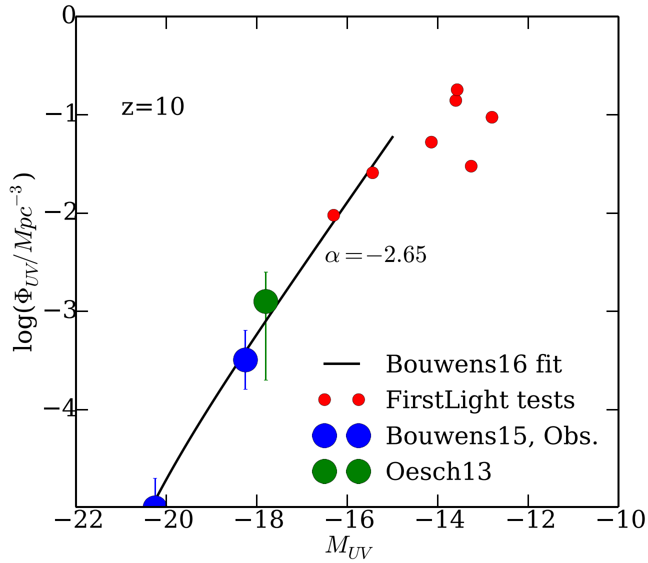

Figure 8. UVLF at $z = 10$. FirstLight and observations (Oesch et al. 2013; Bouwens et al. 2015) give a very steep power-law slope with $\alpha = -2.65$.

regulated by feedback. Therefore, galaxies of a fixed mass live in more massive haloes at lower redshifts.

This evolution does not contradict recent claims of a limited evolution in the SMHM ratio at $z \geq 4$ (Stefanon et al. 2016) because that claim applies only to much higher masses ($M_{\rm vir} \geq 10^{11.5}\,{\rm M}_{\odot}$). That regime is closer to the peak of galaxy efficiency (the highest SMHM ratio), where the relation flattens and shows little evolution with redshift (Behroozi et al. 2013).

Interestingly, at the lowest masses analysed in this paper, $M_{\rm vir} \simeq 10^9$–$10^{9.5}\,{\rm M}_{\odot}$, there is no evolution. This is consistent with Behroozi & Silk (2015) if we extrapolate their $z = 6$ results to lower masses ($M_{\rm vir} \simeq 10^9\,{\rm M}_{\odot}$). This is due to the fact that the relation gets steeper at higher redshifts, mostly driven by the steepening of the halo mass function at these mass scales.

This evolution is absent in most cosmological simulations. For example, the Renaissance simulation (O'Shea et al. 2015; Xu et al. 2016) predicts a much higher stellar fraction (Fig. 6). Their feedback model is not efficient enough to regulate star formation. Therefore, the galaxy growth is mainly driven by the halo growth. This results in too many stars and in a time-independent SMHM ratio.

5 EVOLUTION OF THE UVLF

Fig. 7 shows the UVLF at $z = 8$. The FirstLight results extend the observed function (Bouwens et al. 2015) towards lower luminosities with some overlap at $M_{\rm UV} \simeq -18$. The fit given in Bouwens et al. (2016a), equation (4), provides an excellent description using the same parameters (Table 3). At low luminosities ($M_{\rm UV} > -14$), a flattening of the UVLF is clearly visible. This can be parametrized by equation (5) using $M_{\rm f} = -13.6 \pm 0.2$ and $\delta = 0.4 \pm 0.1$. This flattening is more pronounced than at $z = 6$ (high δ), partially due to the increase in the slope of the UVLF at higher redshifts (higher α).

Fig. 8 shows the UVLF at $z = 10$ from FirstLight and observations (Oesch et al. 2013; Bouwens et al. 2015). All combined results predict a very steep power-law slope for magnitudes brighter than -15 ($\alpha = -2.65 \pm 0.15$). This value is higher than the expected value of -2.27 based on extrapolations of observations at lower redshifts (Bouwens et al. 2015). We predict a faster evolution of the LF slope at $z \geq 10$, in agreement with simple semi-analytical models (Mason, Trenti & Treu 2015) that also predict a similar slope of -2.47 ± 0.26. The main driver of this evolution is just the fast growth and assembly of haloes at these high redshifts.

Due to the large scatter of points at low luminosities ($M_{\rm UV} > -14$), we cannot constrain the flattening of the LF at this redshift. This part of the parameter range will be better covered with the full FirstLight survey.

6 EVOLUTION OF THE STELLAR MASS FUNCTION

Fig. 9 shows the stellar mass function at $z = 8$. The FirstLight tests are consistent with observations (Song et al. 2016) for stellar masses higher than $M_* > 10^7\,{\rm M}_{\odot}$. The simulations extend to lower masses, $M_* = 10^6\,{\rm M}_{\odot}$, and the slope, $\alpha_{\rm s} = -1.85 \pm 0.04$, is close to the lower limit of the observational constraints, -2.2 ± 0.5 (Song et al. 2016). The simulated sample lacks galaxies in the high-mass regime, $M_* > 10^8\,{\rm M}_{\odot}$, at this redshift. Therefore, we cannot exclude a steeper slope at high masses plus a different slope below a stellar mass of $10^{6.5}\,{\rm M}_{\odot}$. Future simulations will clarify this issue.

Finally, Fig. 9 also shows the stellar mass function at $z = 10$. At this redshift, there are no observational estimates. We can predict only the mass function in the low-mass regime, between 10^6 and $10^{7.5}\,{\rm M}_{\odot}$. The low-mass slope does not evolve much between these redshifts, although the normalization is significantly lower at $z = 10$ (Table 4).

7 CONCLUSIONS AND DISCUSSION

We have introduced the FirstLight project, which aims to generate a large data base of simulated galaxies around the epoch of reionization ($z \geq 6$), with an unprecedented numerical resolution (an effective resolution of up to 8192^3 particles). The first tests of this programme, a set of 15 zoom-in, cosmological simulations, yield the following main results:

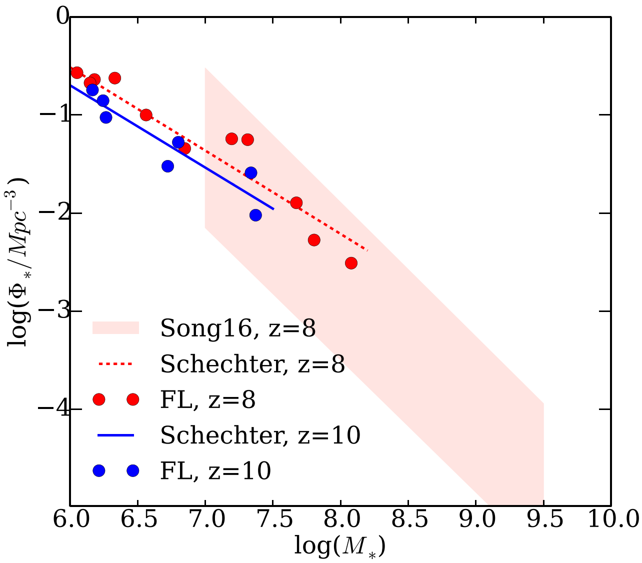

Figure 9. Stellar mass function at $z = 8$ and 10. FirstLight results are consistent with current observations at $z = 8$ (Song et al. 2016), although the slope is slightly lower that the observational estimates, $\alpha_s = -1.85$. The mass function at $z = 10$ shows a similar slope and a slightly lower normalization.

(i) The simulations agree well with the best observational constraints at $z = 6$, such as the UVLF, the stellar mass–UV magnitude relation and the galaxy stellar mass function.

(ii) The UVLF starts to flatten below $M_{\rm UV} > -14$ for haloes with maximum circular velocities of $V = 30$–40 km s^{-1}. This flattening is due to stellar feedback.

(iii) The SMHM relation evolves from $z = 6$ to 10 according to the expectations from abundance matching models (Behroozi & Silk 2015).

(iv) The power-law slope of the UVLF evolves rapidly with redshift, reaching a value of $\alpha \simeq -2.5$ at $z = 10$.

(v) On the other hand, the galaxy stellar mass function evolves slowly with time between $z = 8$ and 10, in particular, at the low-mass end.

The FirstLight project satisfies the need for a large sample of zoom-in calculations with high predictive power for the astrophysical interpretation of the expected wealth of data from new facilities like *JWST*, *WFIRST* and 30-m-class telescopes. A future mock survey of synthetic observations can be directly compared with current and future surveys.

Thanks to the large number statistics, the full FirstLight sample is able to address the mean galaxy properties over a large range of halo masses. It can shed light on the physical origin of the galaxy scaling relations and their evolution during the early galaxy assembly.

The shape of galaxies at high redshifts is very different from local counterparts. They tend to be clumpy, irregular or even elongated (Ceverino, Primack & Dekel 2015). The simulated galaxies will be well resolved, and therefore the mock survey will cover a large diversity of galaxy morphologies. This project will uncover the key mechanisms of morphological transformation, in relation with galaxy efficiency and star formation self-regulation by feedback.

Many physical processes are missing in the current simulations: non-equilibrium cooling, local photoionization and photoheating, radiative transfer effects, and Population III or black hole physics. They are all important in different regimes and situations. Future simulations using the same initial conditions will include some of these effects. However, based on the good agreement between the global properties of the simulated galaxies and current observational constraints, the above physical processes do not seem crucial for the formation of galaxies within the mass and redshift range explored in this paper.

ACKNOWLEDGEMENTS

We thank Peter Behroozi, Joop Schaye and Sandro Tacchella for fruitful discussions. This work has been funded by the ERC Advanced Grant, STARLIGHT: Formation of the First Stars (project number 339177). The authors gratefully acknowledge the Gauss Centre for Supercomputing for funding this project by providing computing time on the GCS Supercomputer SuperMUC at the Leibniz Supercomputing Centre. The authors acknowledge support by the state of Baden-Wirttemberg through bwHPC and the German Research Foundation (DFG) through grant INST 35/1134-1 FUGG.

REFERENCES

Agertz O., Kravtsov A. V., 2015, ApJ, 804, 18
Behroozi P. S., Silk J., 2015, ApJ, 799, 32
Behroozi P. S., Wechsler R. H., Conroy C., 2013, ApJ, 770, 57
Bouwens R. J. et al., 2004, ApJ, 606, L25
Bouwens R. J., Illingworth G. D., Franx M., Ford H., 2008, ApJ, 686, 230
Bouwens R. J. et al., 2015, ApJ, 803, 34
Bouwens R. J., Oesch P. A., Illingworth G. D., Ellis R. S., Stefanon M., 2016a, preprint (arXiv:1610.00283)
Bouwens R. J. et al., 2016b, ApJ, 833, 72
Boylan-Kolchin M., Weisz D. R., Johnson B. D., Bullock J. S., Conroy C., Fitts A., 2015, MNRAS, 453, 1503
Ceverino D., Klypin A., 2009, ApJ, 695, 292
Ceverino D., Dekel A., Bournaud F., 2010, MNRAS, 404, 2151
Ceverino D., Klypin A., Klimek E. S., Trujillo-Gomez S., Churchill C. W., Primack J., Dekel A., 2014, MNRAS, 442, 1545
Ceverino D., Primack J., Dekel A., 2015, MNRAS, 453, 408
Ceverino D., Arribas S., Colina L., Rodríguez Del Pino B., Dekel A., Primack J., 2016, MNRAS, 460, 2731
Cullen F., McLure R. J., Khochfar S., Dunlop J. S., Dalla Vecchia C., 2017, preprint (arXiv:1701.07869)
Dayal P., Ferrara A., Dunlop J. S., Pacucci F., 2014, MNRAS, 445, 2545
Dekel A., Zolotov A., Tweed D., Cacciato M., Ceverino D., Primack J. R., 2013, MNRAS, 435, 999
Duncan K. et al., 2014, MNRAS, 444, 2960
Fiacconi D., Mayer L., Madau P., Lupi A., Dotti M., Haardt F., 2017, MNRAS, 467, 4080
Finkelstein S. L. et al., 2012, ApJ, 756, 164
Finkelstein S. L. et al., 2015, ApJ, 814, 95
Finlator K. et al., 2017, MNRAS, 464, 1633
Genel S. et al., 2014, MNRAS, 445, 175
Gnedin N. Y., 2016, ApJ, 825, L17
Hahn O., Abel T., 2011, MNRAS, 415, 2101
Hopkins P. F., Kereš D., Oñorbe J., Faucher-Giguère C.-A., Quataert E., Murray N., Bullock J. S., 2014, MNRAS, 445, 581
Jaacks J., Thompson R., Nagamine K., 2013, ApJ, 766, 94
Kennicutt Jr R. C., 1998, ARA&A, 36, 189
Klypin A., Zhao H., Somerville R. S., 2002, ApJ, 573, 597
Klypin A. A., Trujillo-Gomez S., Primack J., 2011, ApJ, 740, 102
Komatsu E. et al., 2009, ApJS, 180, 330
Kravtsov A. V., 2003, ApJ, 590, L1
Kravtsov A. V., Klypin A. A., Khokhlov A. M., 1997, ApJS, 111, 73
Liu C., Mutch S. J., Angel P. W., Duffy A. R., Geil P. M., Poole G. B., Mesinger A., Wyithe J. S. B., 2016, MNRAS, 462, 235
Ma X., Kasen D., Hopkins P. F., Faucher-Giguère C.-A., Quataert E., Kereš D., Murray N., 2015, MNRAS, 453, 960
Madau P., Pozzetti L., Dickinson M., 1998, ApJ, 498, 106

Mason C. A., Trenti M., Treu T., 2015, ApJ, 813, 21
Moster B. P., Naab T., White S. D. M., 2013, MNRAS, 428, 3121
O'Shea B. W., Wise J. H., Xu H., Norman M. L., 2015, ApJ, 807, L12
Ocvirk P. et al., 2016, MNRAS, 463, 1462
Oesch P. A. et al., 2013, ApJ, 773, 75
Ostriker E. C., Shetty R., 2011, ApJ, 731, 41
Paardekooper J.-P., Khochfar S., Dalla Vecchia C., 2013, MNRAS, 429, L94
Pallottini A., Ferrara A., Gallerani S., Vallini L., Maiolino R., Salvadori S., 2017, MNRAS, 465, 2540
Pawlik A. H., Rahmati A., Schaye J., Jeon M., Dalla Vecchia C., 2017, MNRAS, 466, 960
Planck Collaboration XVI, 2014, A&A, 571, A16
Rodríguez-Puebla A., Behroozi P., Primack J., Klypin A., Lee C., Hellinger D., 2016, MNRAS, 462, 893
Schaye J. et al., 2015, MNRAS, 446, 521
Song M. et al., 2016, ApJ, 825, 5
Stark D. P., Schenker M. A., Ellis R., Robertson B., McLure R., Dunlop J., 2013, ApJ, 763, 129
Stefanon M., Bouwens R. J., Labbé I., Muzzin A., Marchesini D., Oesch P., Gonzalez V., 2016, preprint, (arXiv:1611.09354)
Stinson G., Seth A., Katz N., Wadsley J., Governato F., Quinn T., 2006, MNRAS, 373, 1074
Stinson G. S., Brook C., Macciò A. V., Wadsley J., Quinn T. R., Couchman H. M. P., 2013, MNRAS, 428, 129
Vogelsberger M. et al., 2014, MNRAS, 444, 1518
Xu H., Wise J. H., Norman M. L., Ahn K., O'Shea B. W., 2016, ApJ, 833, 84
Yue B., Ferrara A., Xu Y., 2016, MNRAS, 463, 1968

This paper has been typeset from a TEX/LATEX file prepared by the author.